

# A NOVEL COMPUTATIONAL METHOD TO COMPUTE ROCK SCOUR DUE TO DAM OVERTOPPING

**ERIK F.R. BOLLAERT<sup>1</sup>**

<sup>1</sup>AquaVision Engineering  
Chemin des Champs-Courbes 1  
CH-1024 ECUBLENS  
SWITZERLAND  
e-mail: erik.bollaert@aquavision-eng.ch

**Key words:** rock scour, computational method, block detachment, case study.

**Summary.** Flood events generating potential risk for dam overtopping may become more frequently in the future, especially because of increasing climate change. Crest overflows at arch dams generally impact the downstream rock mass very close to the dam foundation. As such, any scour of the rock mass generated by this phenomenon may potentially endanger the stability of the dam and its appurtenant structures. Hence, pertinent assessment of this scour formation through space and time is becoming increasingly relevant to dam safety. This paper presents a novel computational method for detachment of prismatic rock blocks from their mass when impacted by high-velocity jets during dam overtopping. The method makes use of the average flow velocities and of block protrusion at the water-rock interface to determine the net uplift pressures and the potential for detachment. Block movements are described based on 1-degree-of-freedom rigid body kinematics applied to submerged bodies and account for the most relevant forces such as quasi-steady and fluctuating lift forces, submerged weight, added mass during block acceleration and potential frictional forces along lateral joints. The paper details the mechanism of block detachment and the way it is accounted for in the computations. Furthermore, an application example of the presented novel approach is outlined through site observed scour formation downstream of a spillway flip bucket.

## 1 INTRODUCTION

This paper presents a novel computational method that has been developed to expand the current state-of-the-art in the field of numerical predictions of scour of rock downstream of dams and in unlined channels. The method incorporates essential physics, such as quasi-steady and fluctuating lift forces, block protrusion and added mass of accelerating blocks, and frictional forces in lateral joints. For plunging turbulent flows, the flow parameters are determined with depth by use of 2D flow matrices. These matrices are defined analytically before start of the scour computations and remain fixed during the computations. As such, an indirect coupling between fluid and rock is obtained. The here presented novel method, together with other existing and novel approaches (see Bollaert, 2021) have been implemented on a cloud-based platform. As such, users are able to apply and compare a wide range of methods within one environment, based on customized parametric settings of dam, flow and rock mass.

Moreover, a digital database platform has been developed complementary to the software platform, allowing to freely consult any type of worldwide rock scour case studies that have been performed and published, either real-life or laboratory generated. This platform aims at

offering a practical and continuously updated database with the potential of informing specialists and engineers on the most relevant results, parameters and calibrations that have been used for each of the available scour computational methods.

## 2 PLUNGING 2D JET FLOWS

### 2.1 Concept

The hydraulic parameters of 2D plunging jet flows (see Figure 1) are determined analytically along the initial water-rock interface and vertically down into the rock mass, and are stored as 2D matrices used by the software during the computations.

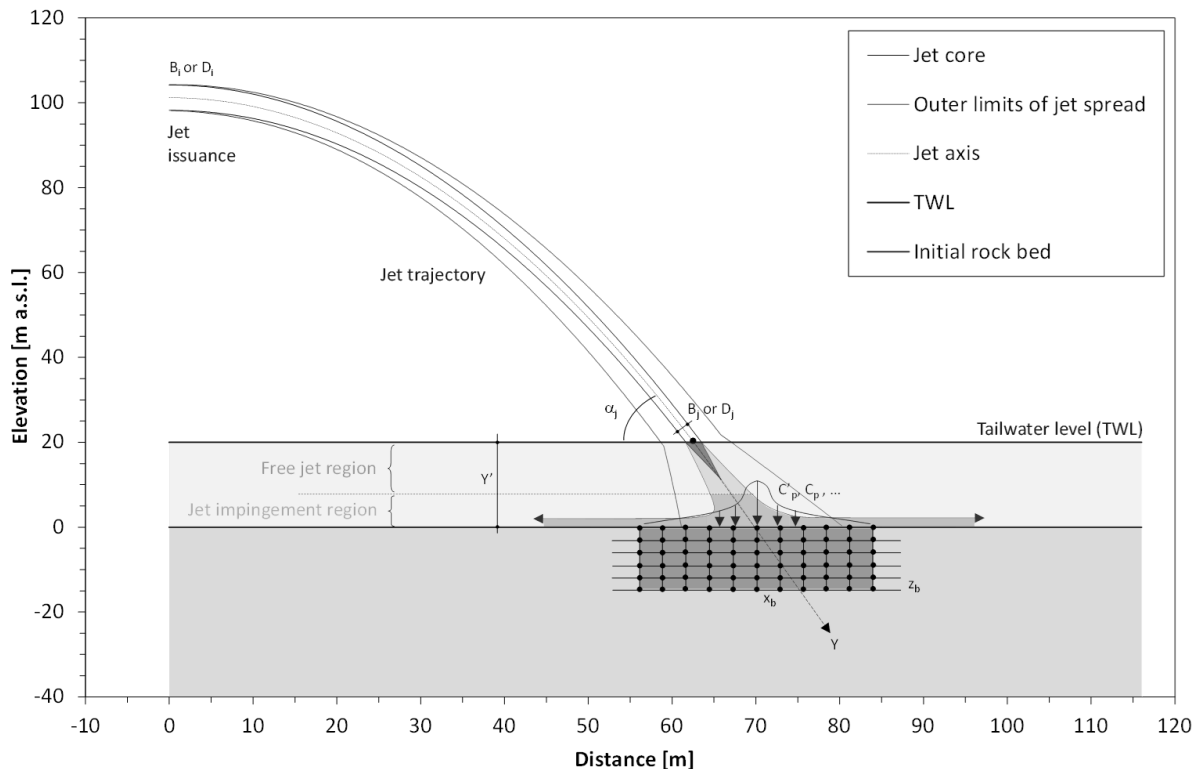


**Figure 1.** Sketch of obliquely plunging turbulent flow diffusing through plunge pool and impacting the water-rock interface (source: rocsc@r Technical Manual, 2022).

### 2.2 2D flow matrices

The equations describing plunging turbulent flows allow predefining and storing the values of the hydraulic parameters in 2D matrices. These respect the network of computational nodes of the 2D vertical profiles, along which the scour computations are being performed (Figure 1).

As such, in every computational node, the hydraulic parameters that are needed for the scour computations are being predefined before start. The analytical equations assume a quasi-horizontal and quasi-flat interface between the rock and the water, without any perturbing elements or suddenly changing interface shapes. The corresponding values account for the progressively increasing flow depth during scour formation. As such, the following hydraulic parameters are predefined with depth and stored in 2D matrices:

**Table 1.** List of hydraulic parameters pre-defined in 2D flow matrices.

Parameter	Description
$C_p$	Mean dynamic pressure coefficient
$C'_p$	Fluctuating (RMS) dynamic pressure coefficient
$C_{max}$	Maximum dynamic pressure coefficient
CI	Dynamic impulsion coefficient
VEL (MQSI)	Average flow velocity quasi-parallel to interface
SP	Average stream power at interface

The pressure coefficients have to be multiplied by  $\rho V^2/2g$  to obtain the pressure values in  $[N/m^2]$ , and the impulsion coefficient by  $\rho AV^2L/c$  to obtain impulsions in  $[Ns]$ , with  $V$  the jet velocity at impact in the pool (m/s),  $c$  the wave celerity (m/s),  $L$  the joint length (m) and  $A$  the horizontal rock block area ( $m^2$ ). Figure 2 illustrates an example of the determination of the average dynamic pressure coefficient  $C_p$  at the water-rock interface, due to an obliquely impacting rectangular jet. The jet impacts the pool at point C under an angle of about  $70^\circ$  with the horizontal, and the stagnation point of the jet at the water-rock interface is at R. The spatial distribution of the pressure at the rock surface is represented by the black curve (right-hand side axis), while the evolution with depth is represented by a graded heatmap (legend on the right).

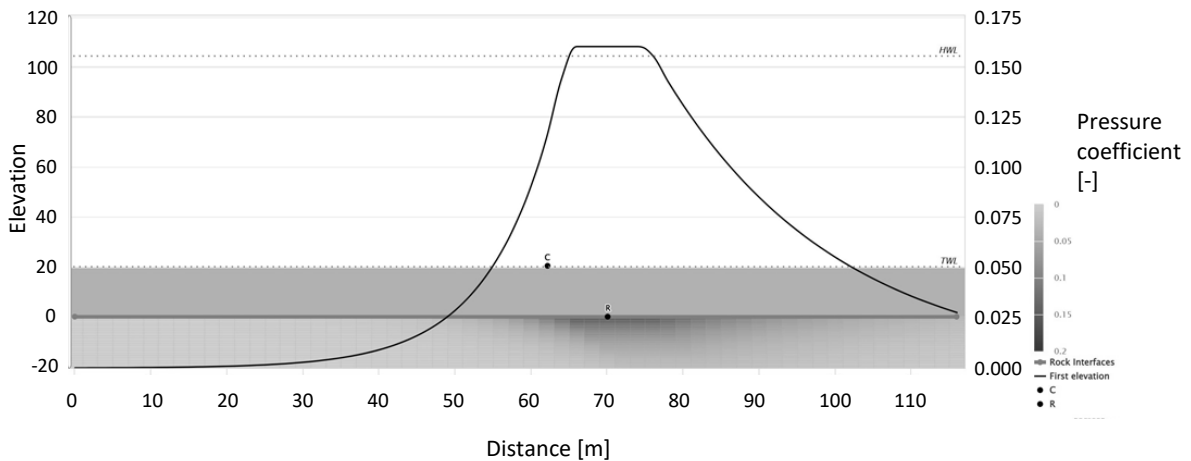


**Figure 2.** Example of 2D determination of average dynamic pressure at water-rock interface generated by an obliquely impacting jet (source: rocsc@r 2022).

Similar curves are defined for all hydraulic parameters listed in Table 1. This 2D matrix system covers both circular and rectangular-shaped jets, as well as vertically or obliquely impinging jets for angles between  $20$  and  $90^\circ$ . Moreover, both compact and broken-up jets are accounted for, as well as the air concentration and degree of break-up of the jets at impact, and the initial turbulence intensity at issuance from the dam.

### 3 QUASI-STEADY IMPULSION METHODS

#### 3.1 The QSI method (Bollaert, 2012)

The QSI method developed by Bollaert (2012) computes the scour potential along the water-rock interface, from the point of jet impingement laterally outwards, based on wall jet velocities. Prismatic rock blocks are checked for detachment or peeling off by sudden deviation of the wall jet flow due to block protrusion, generating a quasi-steady net lift force on the block (see Figure 3). It follows a sequence of computational steps as presented in Figure 5.

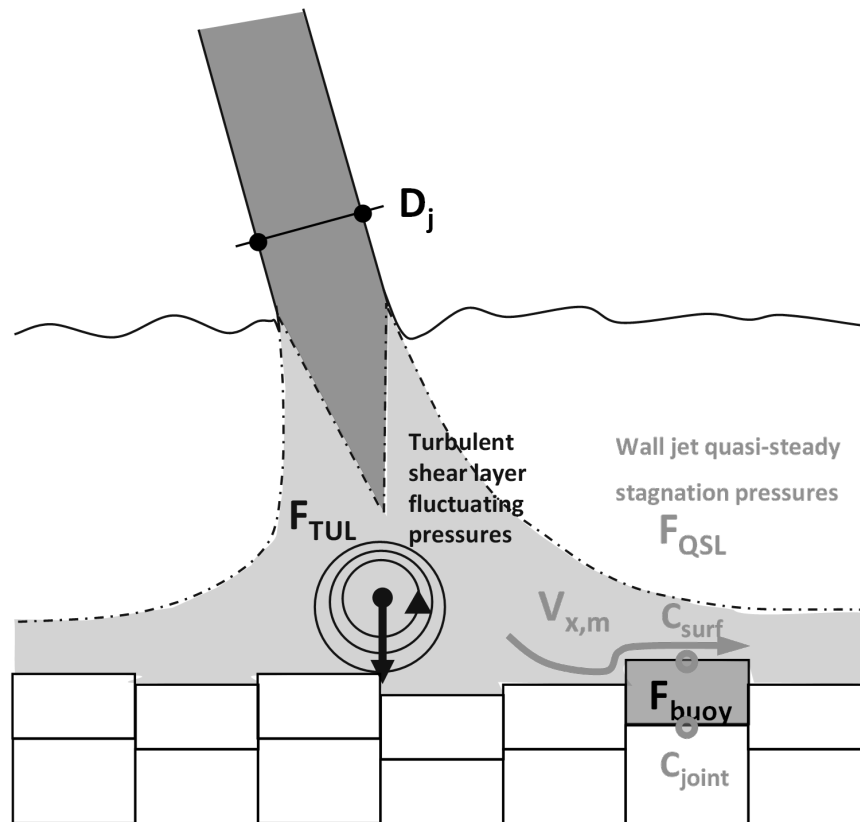


**Figure 3.** Protruding prismatic rock blocks detached by quasi-steady impulsion (Bollaert, 2012).

Subsequent to quasi-2D diffusion of jets, the water-rock interface deflects the jets towards up- and downstream. This quasi-steady flow parallel to the bottom may then be potentially deviated by protruding rock blocks, generating quasi-steady net uplift forces on these blocks. This allows defining the scour hole and the risk for regressive scour towards the dam toe.

Quasi-2D jet diffusion in the free jet region has self-preserving velocity and pressure profiles and is not influenced by the presence of the pool bottom. Several researchers have studied the velocity and pressure distributions in this area (Rajaratnam (1976), Hartung & Hausler (1973), Bohrer et al. (1998)). Most studies relate the axial jet velocity decay to the local jet thickness or diameter or to the inverse of the water depth  $Z$ . For compact jets, the equation expressing  $V(Z)$  as a function of the velocity at impact in the pool  $V_i$ , is illustrated at Figure 4.

The core of the jet has a constant velocity and is generally taken at 4-5 times the jet thickness at impact. The flow velocity at the point of jet deflection at the interface, i.e.  $V_{Z_{bottom}}$ , is used as initial velocity to define the velocity decay along the wall jet regions up-and downstream.

Second, the wall jet region describes the flow parallel to the bottom, outside of the impingement region. In case of protruding rock blocks, the flow is deflected, which generates lift and drag forces. These forces are mostly of quasi-steady character (Bollaert and Hofland, 2004), although some fluctuations generally exist. The deflection of the jet occurs in both up- and downstream directions, depending on the angle of the jet upon impact. Based on Reich (1927), plane jets with discharge  $q_{total}$  and thickness  $D_j$  impinging on a flat plate under an angle  $\delta$  subdivide the discharges and thicknesses as follows:

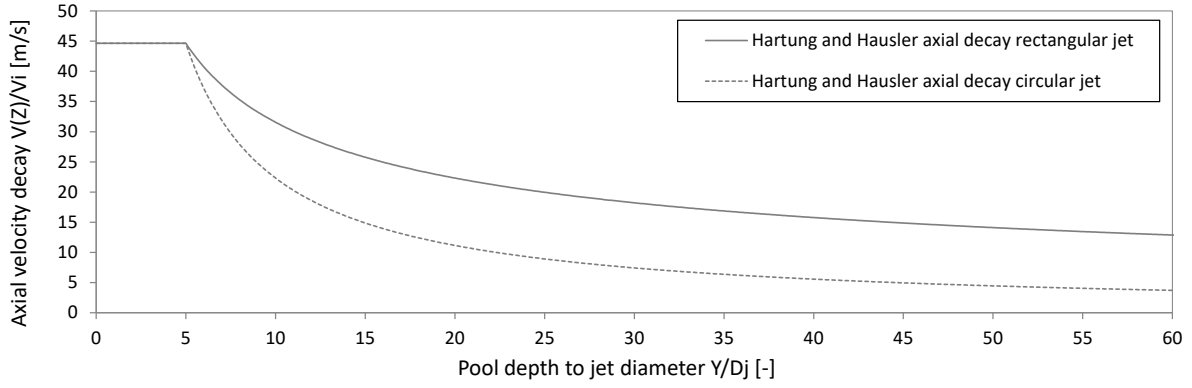


**Figure 4.** Axial jet velocity decay for circular and rectangular-shaped jets.

$$\frac{q_{\text{up}}}{q_{\text{total}}} = \frac{h_{\text{up}}}{D_j} = \frac{1}{2} \cdot (1 - \cos \delta) \quad (1)$$

$$\frac{q_{\text{down}}}{q_{\text{total}}} = \frac{h_{\text{down}}}{D_j} = \frac{1}{2} \cdot (1 + \cos \delta) \quad (2)$$

Wall jets are characterized by their initial flow velocity  $V_{Z_{\text{bottom}}}$  and their initial thickness  $h_{\text{up/down}}$  at the point of deflection. Initiating from this location, wall jets develop radially outwards following self-preserving velocity profiles (Beltaos & Rajaratnam, 1973) as follows:

$$\frac{V_{X,\text{max}}}{V_{Z,\text{bottom}}} = \min \left( V_{Z,\text{bottom}}, \frac{3.5}{\sqrt{\frac{X}{h_{\text{up/down}}}}} \right) \quad (3)$$

in which  $V_{Z_{\text{bottom}}}$  depends on the diffusion angle of the impinging jet and on its development length through the water depth  $Z$ , based on equations (1) and (2).  $V_{Z_{\text{bottom}}}$  continuously changes during scour formation.  $V_{X,\text{max}}$  expresses the decay of the maximum cross-sectional jet velocity with the relative distance from the start of the wall jet (lateral distance  $X$  divided by the initial thickness of the deflected jet  $h_{\text{up/down}}$ ). The related lift forces are defined by an uplift coefficient  $C_{\text{uplift}}$  expressing the pressure as a function of the kinetic energy  $V^2/2g$  of the quasi-parallel flow. Based on Reinius (1986), net uplift coefficients are between 0 and 0.5, depending on the degree of protrusion and the shape of the blocks. For the computations, coefficients of 0.1-0.2 are plausible for low to very low protrusions, while coefficients of 0.3-0.5 correspond to moderate to significant protrusions, i.e. for rough and irregular pool bottoms. The latter values are considered most plausible for a real water-rock interface. Finally, based on block shape and dimensions, block stability under quasi-steady flow impact is computed by defining the net uplift force  $F_{\text{net}}$  during jet impact, by accounting for the submerged weight of the block as stabilizing force. The stability of the block is expressed by the following force-balance equation:

$$F_{\text{net}} < 0 \quad (4)$$

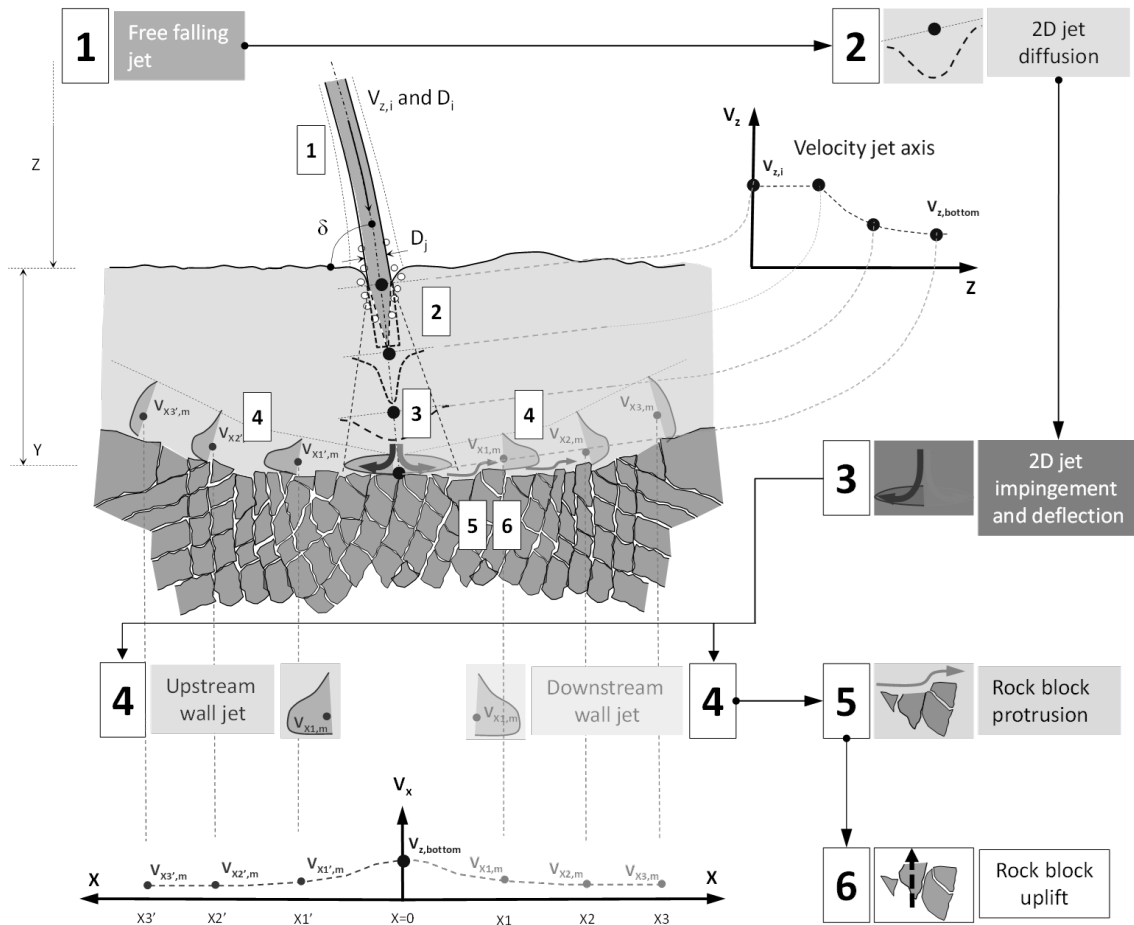


Figure 5. Sketch of computational methods used by quasi-steady impulsion (Bollaert, 2012).

### 3.2 The MQSI method (Bollaert, 2021)

#### 3.2.1 Introduction

The QSI method developed by Bollaert (2012) has been modified within the framework of the rocscor® software by adding the following aspects:

- additional shear forces in the lateral joints generated by net pressure differences acting on the upper and lower vertical faces (i.e. lateral joints) of the block
- additional pulsating lift forces, valid during a limited time duration, and superposed to the time-averaged (quasi-steady) component of the lift force
- wall jet velocity decay valid for circular-shaped jets and broken up jets
- wall jet velocity decay valid for jets impacting the plunge pool under an oblique angle, for both circular and rectangular-shaped jets, and expressed as a function of the jet thickness at impact

It is named the MQSI (Modified QSI) method (Bollaert, 2021) and checks for block stability by considering both quasi-steady and additional pulsating lift forces on prismatic blocks:

- *STEP 1: quasi-steady lift forces*  
Block stability criterion according to equation (4), i.e. a net force balance is checked for by only considering quasi-steady forces. In case the block is unstable, no second step is being checked for and the computation ends. In case the block is stable, go to STEP 2.

- *STEP 2: total lift forces*

Block stability criterion according to the procedure of net uplift height given to the block based on the net total lift force and its time duration. The total net lift force is composed of a quasi-steady part (STEP 1) and of a single pressure pulse of duration  $\Delta t_{\text{pulse}}$  that is superposed to the quasi-steady lift force. In case the total net lift force is positive, application of a critical uplift height criterion to determine block detachment or stability, as detailed in Bollaert (2021). In case the total net lift force is still negative, the computation ends and the block is considered stable.

### 3.2.2 Quasi-steady forces on a protruding block

The quasi-steady net force  $F_{\text{net}}$  ([N]) acting on a protruding prismatic block is decomposed into net dynamic uplift forces acting on the block ( $F_{\text{under}} - F_{\text{over}}$ ), buoyancy forces  $F_{\text{buoy}}$ , gravity forces  $F_{\text{grav}}$ , shear forces along the vertical joints based on weight and buoyancy ( $F_{\text{sh,G}}$ ) and finally shear forces based on differential pressures along the upstream and downstream vertical faces of the block ( $F_{\text{sh,P}}$ ). The net lift force  $F_{\text{net}}$  can be written as follows:

$$F_{\text{net}} = F_{\text{under}} - F_{\text{over}} + F_{\text{buoy}} - F_{\text{grav}} - F_{\text{sh,G}} - F_{\text{sh,P}} \quad (5)$$

The quasi-steady water pressure forces that act along the upper and lower faces of the prismatic block generate a lift force on the block. The average value of this lift force is essential to the analysis. It is determined by using a time-averaged net uplift pressure coefficient  $C_{\text{up,QSI}}$  that is computed based on the time-averaged dynamic pressure coefficients (i.e. pressures that are non-dimensionalized based on the energy at impact of the jet  $\rho V_j^2/2$ ) acting on both the surface ( $C_{\text{over}}$ ) and the bottom ( $C_{\text{under}}$ ) of a prismatic rock block:

$$C_{\text{up,QSI}} = C_{\text{under}} - C_{\text{over}} \quad [-] \quad (6)$$

CASE	$C_{\text{up,QSI}}^*$				$\text{MULT} \cdot C_{\text{up,QSI}}^{**}$			
	min	max	avg	remark	min	max	avg	remark
1	0.00	0.10	0.05		0.00	0.00	0.00	
2	0.10	0.15	0.12		---	---	---	
3	0.70	0.90	0.80		---	---	---	
4	0.10	0.40	0.25	$0.9 \sqrt{\frac{k}{Z_b}}$	0.025	0.11	0.07	$0.24 \sqrt{\frac{k}{Z_b}}$
5	0.10	0.20	0.15	approx.	---	---	---	
6	0.08	0.09	0.08		---	---	---	
7	0.30 0.40	0.35 0.50	0.32 0.45	$h/k \sim 4-9$ $h/k \sim 1-2$	---	---	---	
8	-0.07 -0.12	-0.07 -0.20	-0.07 -0.16	$h/k \sim 4-9$ $h/k \sim 1-2$	---	---	---	

(for cubical blocks and  $0.01 < k/Z_b < 0.2$ )  
\* based on quasi-steady net uplift pressures/forces

(for cubical blocks and  $0.01 < k/Z_b < 0.2$ )  
\*\* based on RMS values of net uplift forces

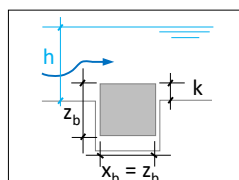
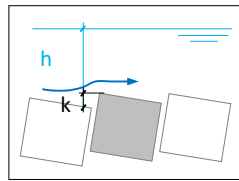
**Figure 6.** Overview of dynamic pressure coefficients for different block situations adapted from Reinius (1986) and Pells (2016) (Bollaert, 2021).

Based on experiments performed by Reinius (1986) and Pells (2016), 8 geometrical cases of a prismatic rock block and its surrounding rock mass have been documented. For each case, the range of minimum, maximum and average differences between the bottom and surface pressure coefficients are defined in Figure 6. For case 4, a mathematical equation is available to express the net pressure difference. This equation is based on net uplift force measurements on protruding cubic blocks (Pells, 2016), by using the horizontal block surface  $x_b, y_b$  as a reference. The parameters  $z_b$  (block height = block side-length) and  $k$  (block protrusion) of this equation are illustrated in Figure 7.

The quasi-steady lift forces are then expressed by use of a dynamic uplift pressure coefficient  $C_{up,QSI}$  as follows:

$$F_{up,QSI,AVG} = F_{under} - F_{over} = C_{UP,QSI} \cdot \rho_w \cdot x_b \cdot y_b \cdot \frac{V_j^2}{2} \quad (7)$$

CASE	$C_{UVF} - C_{DVF}$			
	min	max	avg	eq.
1	0.00	0.00	0.00	
2	0.00	0.00	0.00	
3	0.80	0.90	0.85	
4	0.05	0.30	0.15	$0.67 \sqrt{\frac{k}{z_b}}$
5	0.20	0.30	0.25	
6	-0.25	-0.25	-0.25	
7	0.01 -0.20	0.05 -0.10	0.03 -0.15	$h/k \sim 5-10$ $h/k \sim 2-4$
8	0.00	0.00	0.00	

(for cubical blocks and  $0.01 < k/z_b < 0.2$ )  
\* based on quasi-steady lateral pressures/forces

**Figure 7.** Net lateral pressure differences along lateral joints of blocks for different block situations adapted from Reinius (1986) and Pells (2016) (Bollaert, 2021).

Quasi-steady water pressures also act in joints that are located along the upstream and downstream vertical (or quasi-vertical) faces of the prismatic rock block. When these pressure forces in the lateral joints are not equal, i.e. when a net lateral pressure difference is generated that laterally pushes the block towards its neighboring block, a shear force is generated that is opposed to vertical block movement.

The initial shear forces that may exist in these lateral joints by natural roughness and contact points are considered negligible due to the progressive opening and/or widening of these joints by vibrational movements of the rock block during jet impingement.

Accounting for a rock joint friction angle  $\varphi$ , this generates a quasi-steady shear force  $F_{sh,p}$  in one of the lateral joints, by expressing the lateral water pressures by means of average pressure coefficients  $C_{UVF}$  (upstream vertical face) and  $C_{DVF}$  (downstream vertical face) as follows:



$$F_{sh,P} = ABS((C_{UVF} - C_{DVF}) \cdot \rho_w \cdot z_b \cdot y_b \cdot \frac{V_j^2}{2} \cdot \tan(\varphi)) \quad (8)$$

Similar to the pressures over and under the block, experiments performed by Reinius (1986) and Pells (2016) allowed documenting 8 geometrical cases of a prismatic rock block and its surrounding rock mass. For each case, the range of minimum, maximum and average differences between the lateral pressure coefficients is defined in Figure 7. For case number 4, a mathematical equation is available to express this net lateral pressure difference. It may be observed that, on the average, these pressure differences are rather low to very low. Hence, during the computations, safe-side assumptions of low to quasi-zero values are recommended.

In addition to shear forces generated by differential water pressures inside lateral joints, an additional shear force may occur for blocks that have a non-zero angle of orientation with the horizontal. In such a case, the component of the gravity force that is oriented perpendicular to the lateral joint will add a shear force  $F_{sh,G}$  in the joint by accounting for the rock joint friction angle  $\varphi$ . In the same way, the component of the buoyancy force that is oriented perpendicular to the lateral joint will reduce this added shear force. Finally, similar to the QSI method, block stability under quasi-steady forces is obtained by applying a force-balance equation (4).

### 3.2.3 Pulsating forces on a protruding block

Second, the fluctuating part of the lift forces on a protruding prismatic block can be described by the RMS pressure fluctuation coefficient  $C'_{up,QSI}$  of the pressure acting at the location of block protrusion (i.e. over the upper face of the block):

$$C'_{up,QSI} = \frac{\text{RMS (local pressure at block protrusion)}}{\rho \cdot \frac{V_j^2}{2}} \quad [-] \quad (9)$$

Similar to the MDI (Bollaert, 2021) method, and based on experiments by Federspiel (2011), Bollaert (2021) related the fluctuating net uplift pressure coefficient  $C_{up,block}$  to the RMS pressure fluctuations at the block surface  $C'_{up,QSI}$  by means of a multiplication factor MULT :

$$\text{MULT} = \frac{C_{up,block}}{C'_{up,QSI}} \quad [-] \quad (10)$$

The  $C_{up,block}$  values can be estimated from local pressure and lift force recordings by Pells (2016) for cubical blocks with or without protrusion and are presented in the last column of Figure 4. The fluctuating lift force on the block  $F_{up,QSI,RMS}$  can then be written as:

$$F_{up,QSI,RMS} = \text{MULT} \cdot C'_{up,QSI} \cdot \rho_w \cdot x_b \cdot y_b \cdot \frac{V_{x,max}^2}{2} \quad [N] \quad (11)$$

Typical values for MULT are of 4.0-4.5. As described in detail in Bollaert (2021), the MQSI method makes use of the time durations of the pressure pulses to transform fluctuating lift forces into net lift impulsions. Typical durations for laboratory joints are of 0.10 sec. For real-life joints at prototype scale, however, time durations may become longer in case of very long joints, and are determined by the resonance frequency of the joints around the blocks, based on the following equation valid for open-ended joints:

$$\frac{1}{f_{\text{res}}} = \Delta t = \frac{2L}{c} \quad (12)$$

Furthermore, net pressure differences along both the upstream and downstream vertical faces of a block have been included in the uplift analysis. Corresponding coefficients are summarized in 7. Finally, similar to the MDI method, added mass has been included.

### 3.2.4 Total forces on a protruding block

By superposing the fluctuating lift force to the time-averaged lift force, the total lift force  $F_{\text{net,QSI}}$  is then written:

$$F_{\text{net,QSI}} = F_{\text{up,QSI,AVG}} + F_{\text{up,QSI,RMS}} = (C_{\text{up,QSI,AVG}} + \text{MULT} \cdot C'_{\text{up,QSI}}) \cdot \rho_w \cdot x_b \cdot y_b \cdot \frac{V_{X,\text{max}}^2}{2} \quad (13)$$

Finally, block detachment is then expressed by means of a critical net uplift height of the block  $n_b = h_{\text{up}}/z_b$ , with  $h_{\text{up}}$  the total uplift height given to the block and  $z_b$  the total block height. Typical values for  $n_b$  are of 0.10 – 0.50 (Bollaert, 2021).

## 4 CASE STUDY

### 4.1 Site and project

The Chucás hydroelectric project, owned by Enel Costa Rica, was developed as a BOT project (Figure 8, Capuozzo & Jiménez, 2017). It is located about 40 km west of San José, the country's capital. The project, in operation since November 2016, dams the Tárcoles river with a 63 m high dam. A surface penstock, about 400 m long and 6.5 m in diameter, leads to a powerhouse where two Francis units generate a total output of 50 MW.

For flood control, the dam is equipped with four radial gates, 15 m by 12.4 m, capable of discharging 5400 m<sup>3</sup>/s under design conditions (Capuozzo & Jimenez, 2017). This large discharge is conveyed through a ski-jump spillway chute discharging into the rock bed downstream of the dam. Scour formation in this unprotected rock mass was expected and a pre-excavation was planned but never executed. The corresponding plunge pool formation, in this particular case, may endanger the exposed penstock, because of the risk of lateral expansion of the scour hole, which might affect this structure. In addition, there is the risk that backwards erosion of the plunge pool may affect the dam foundations.

### 4.2 Geology

Based on Capuozzo & Jiménez (2017), the in-situ rock mass consists of volcanic rocks such as andesitic lava, ignimbrite pyroclastic flows and occasionally thin layers of tuff and ash deposits. Good outcrops are observed on both banks of the river, however, the bedrock cannot be observed as a result of the constant flow of the river. The rock mass consists of aphanitic (fine grain) and aphanitic porphyritic (coarse grain) andesitic lava flow. The aphanitic mass is hard and highly fissured, and has good weathering resistance. The aphanitic porphyritic contains abundant calcite giving a brecciated textured appearance (called the 'coarse grain'), it is soft to moderately hard, moderately fissured andesite, susceptible to weathering. The rock mass has been affected by a hydrothermal process, which has made it very susceptible to accelerated weathering when exposed to the environmental conditions of the area (rain and

sun).

Local site investigation with boreholes indicates a variable rock quality designation (RQD), however, at the left abutment the rock is more fissured. The RQD percentage at the left abutment ranges from 0 to 76 per cent with an overall average of 40 per cent, which classifies the rock mass as poor quality.

The joint spacing produces flat-shaped rock blocks of only 0.04 to 0.5 m sidelength. These results would indicate that a plunge pool formation is very likely to occur relatively rapidly. As the smaller range of values correspond to gravel and cobbles generated by ball-milling, only a block sidelength of 0.5 m has been used, together with a height-to-sidelength ratio of 1:2.

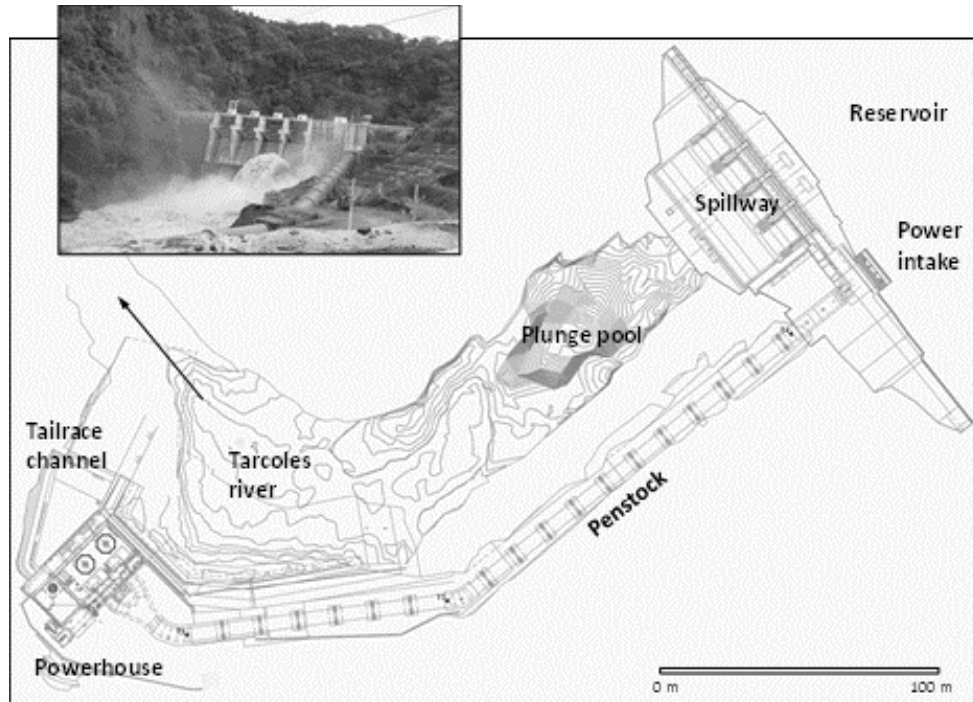


Figure 8. General layout of Chucàs HEP (source: O. Jiménez).

### 4.3 Tropical storm

Based on Capuozzo & Jiménez (2017), the tropical storm Nate hit Costa Rica between 4 and 6 October 2017. The storm remained almost stationary for two days, close to the Caribbean coast of Costa Rica, displacing humidity from the Pacific Ocean toward the dam's watershed. Rain fell for 48 hours, reaching precipitation levels of between 200 to 400 mm over the whole basin of the Chucàs powerplant. As a result, peak flows of more than 3000 m<sup>3</sup>/s were discharged through the radial gates, starting in the early hours of 5 October and lasting for about 24 hours. According to the records, this flood has a return period of more than 100 years.

Although the powerplant suffered relatively little damage, and was back in operation after two days, it was clear that important scour downstream of the dam had taken place because of the natural formation of the plunge pool. Bathymetric measurements showed that a plunge pool had been formed, with a maximum depth of 25 m, larger than the 20 m initially assumed based on hydraulic model tests. Fortunately, the observed damage and scour did not pose threats to the existing structures. It was estimated that about 15'000 m<sup>3</sup> of material was removed and deposited downstream.

#### 4.4 Numerical reproduction of observed scour

The scour formed during tropical storm Nate has been numerically reproduced. The maximum observed discharge of  $3'000 \text{ m}^3/\text{s}$  has been used for the scour computations. These computations are based on quasi-steady detachment and displacement towards downstream of rock blocks (QSI and MQSI methods). For the MQSI method, a succinct parametric analysis has been performed of the net uplift pressure coefficient  $C_{\text{up,QSI}}$  and of potential drag forces inside the lateral joints ( $C_{\text{drag}} = C_{\text{UVF}} - C_{\text{DVF}}$ ), as explained in § 3.2.2. For the QSI method, no parametric analysis was performed.

Figure 9 illustrates the scour computed by the QSI and MQSI computational methods. The best-fit between computations (grey lines) and site observations (black line) was obtained for a  $C_{\text{up}}$  coefficient equal to 0.30 and no drag forces inside the lateral joints. Variations involving  $C_{\text{up}} = 0.20$  and  $0.40$  and  $C_{\text{drag}}$  values of  $0.00 - 0.10$  did not profoundly change the outcome of the estimate, but slightly decrease or increase the potential compared to site observations. Also, the QSI method ( $C_{\text{up}} = 0.40$ ) revealed to be in good agreement with the MQSI method.

In general, both scour hole depth and shape, especially towards upstream, are soundly reproduced by the numerical modelling. The computed downstream slope slightly deviates from the observed one, which might be due to the rock block deposits that were observed after the flood in the downstream river, which are not taken care of in the numerical model.

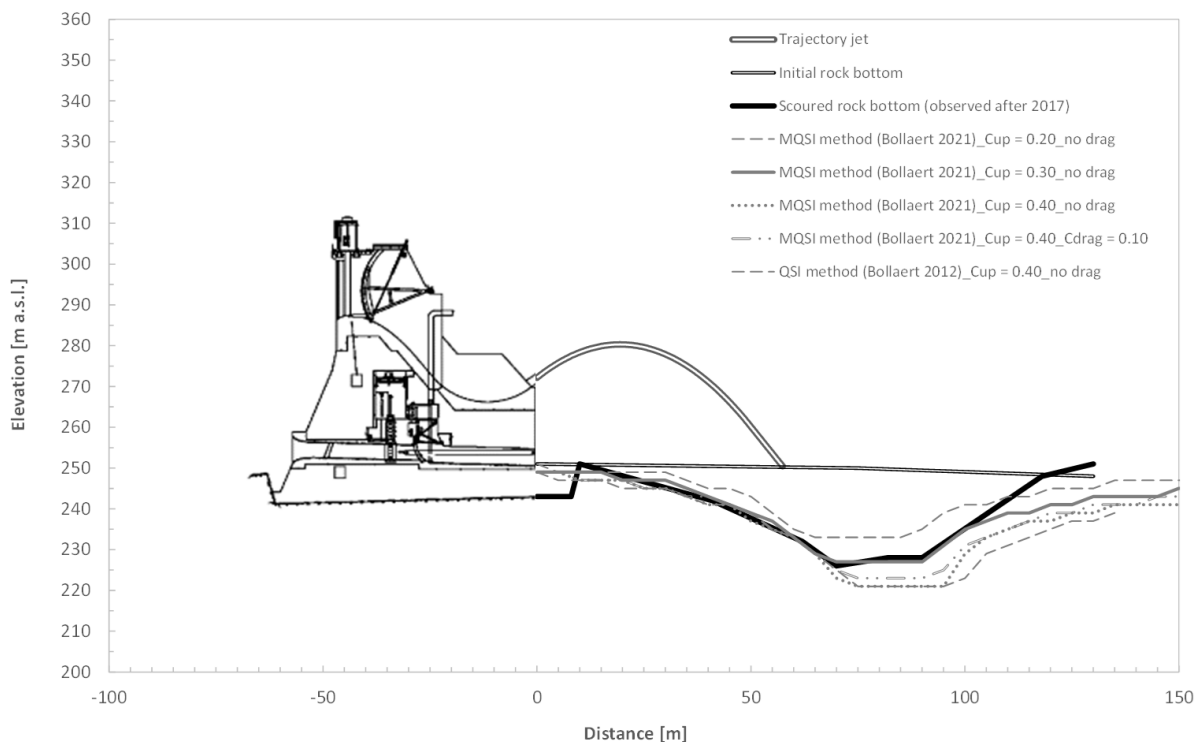


**Figure 9.** Scour potential computed at Chucàs HEP by MQSI and QSI methods.

Figure 10 illustrates the flow velocities stored in 2D flow matrices at start of the computations. The grey-colored heatmap provides the evolution of velocities with depth, while the black curve expresses the axis value and radial decay of the flow velocity along the water-rock interface.

## 5 CONCLUSIONS

This paper presents a novel computational method to expand the current state-of-the-art in the field of numerical predictions of scour of rock downstream of dams and in unlined channels and stilling basins. The method incorporates additional physics, such as quasi-steady and fluctuating lift forces on protruding blocks, added mass of moving blocks and frictional forces in lateral joints, and relies on a 2D determination of the most relevant turbulent flow parameters by use of 2D flow matrices that store the relevant flow parameters with depth. These matrices are defined at start of the computations and remain fixed during the computations.

The novel MQSI method, together with other existing and novel approaches (Bollaert, 2021) has been implemented on a cloud-based software platform. This next-gen software platform procures physics-based scour estimates using a series of 2D vertical profiles, allowing for a quasi-3D reconstitution of the scour hole. It is based on a 2D assessment of the geo-mechanical characteristics of the rock mass with depth. As such, users are able to apply and compare a wide range of methods within one environment, based on customizable parametric settings of the dam, the turbulent flow and the rock mass.

The QSI and MQSI methods were applied to a ski-jump jet generating scour observed in the unprotected rock downstream of Chucàs Dam in Costa Rica during a 2017 tropical storm event (return period of about 100 years). Both methods allow sound numerical reproduction of the observed scour, although the novel MQSI method seems slightly more pertinent. Parametric analysis points out the most relevant values for to be considered for practice.

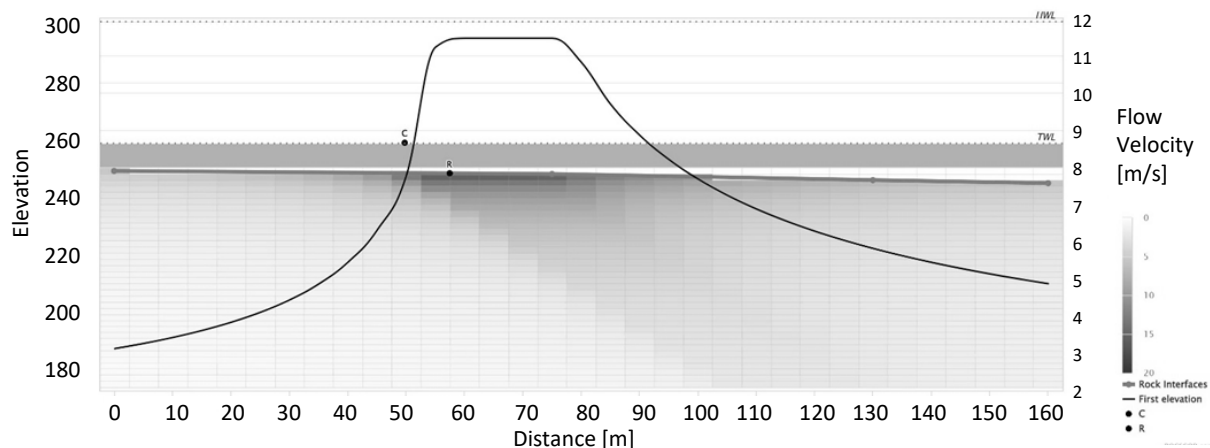


**Figure 10.** Average flow velocities at water-rock interface as computed at Chucàs HEP.

## ACKNOWLEDGEMENTS

Sincere thanks go to M. O. Jiménez from DLZ Carbon Ingenieria for his kind transmission of the photos and the hydraulic and geologic information needed to correctly perform the scour computations.

## REFERENCES

Bohrer, J.G., Abt, S.R. and Wittler, R.J. (1998). “Predicting plunge pool velocity decay of free falling, rectangular jet.” *Journal of Hydraulic Engng, ASCE*, Vol. 124, N° 10, pp. 1043-1048.

Bollaert, E.F.R. (2002). "The influence of plunge pool air entrainment on the presence of free air in rock joints." Proceedings of the International Workshop on Rock Scour, September 25-28 2002, EPFL, Lausanne, Switzerland.

Bollaert, E.F.R. (2012). "Wall Jet rock scour in plunge pools: a quasi-3D prediction model." Intl. Journal on Hydropower & Dams, 2012.

Bollaert, E.F.R. (2021). "The rocsc@r™ cloud: An innovative digital platform to compute and record rock scour." Intl. Journal on Hydropower and Dams, Issue 5.

Bollaert, E.F.R. (2022). "rocsc@r Technical Manual". Internal Report. AquaVision Engineering Sàrl, Ecublens, Switzerland.

Bollaert, E.F.R. and Hofland, B. (2004). "The Influence of Flow Turbulence on Particle Movement due to Jet Impingement." 2nd Scour and Erosion Conference, Singapore, November 2004.

Bollaert, E.F.R. and Schleiss, A.J. (2005). "A physically-based model for evaluation of rock scour due to high-velocity jet impact." Journal of Hydraulic Engineering, March 2005.

Bollaert, E.F.R., Federspiel, M., Schleiss, A. (2013). "The influence of Added Mass on Rock Block Uplift in Plunge Pools." IAHR Congress, Chengdu, China.

Capuozzo, L. and Jiménez, O. (2017). "Model and prototype studies for the Chucàs hydro scheme Costa Rica." Intl. Journal of Hydropower and Dams, Issue 6.

Federspiel, M. (2011). "Response of an Embedded Block Impacted by High-Velocity Jets." PhD EPFL N°5160.

Federspiel, M., Bollaert, E.F.R., Schleiss, A.J. (2011). "Dynamic Response of a Rock Block in a Plunge Pool due to Asymmetrical Impact of a High-velocity Jet." 34th IAHR World Congress, Brisbane.

Hartung, F. and Hausler, E. (1973). "Scours, stilling basins and downstream protection under free overfall jets at dams." Proceedings of the 11th Congress on Large Dams, Madrid, pp.39-56.

Liu, P.Q., Dong, J.R. and Yu, C. (1998). "Experimental investigation of fluctuating uplift on rock blocks at the bottom of the scour pool downstream of Three-Gorges spillway." Journal of Hydraulic Research, IAHR, Vol. 36, N°1, pp. 55-68.

Pells S. (2016). "Erosion of rock in spillways." Ph.D. thesis, UNSW Australia, Kensington, NSW, Australia.

Rajaratnam (1976). Turbulent Jets. Developments in Water Science, Elsevier.

Reich, F. (1927). "Umlenkung eines Freien Flüssigkeitsstrahles an einer ebenen Platte." Zeitschrift VDI 71 (8): p. 261-264.

Reinius, E. (1986). „Rock Erosion.“ Intl. Water Power and Dam Construction, 38(6): p. 43-48.